On the Lifetime-Equivalent Defect Density: Properties, Application, and Pitfalls

Axel Herguth

***Abstract*—The basic idea, derivation, and definition of the lifetime-equivalent defect density (alternatively termed as effective, relative, or normalized defect density) in the context of studies on changes of bulk excess charge carrier lifetime in crystalline silicon is presented, and the general dependencies on injection and temperature are discussed. As the concept of lifetime-equivalent defect density is often applied to light-induced phenomena, the application to boron–oxygen-related light-induced degradation and regeneration is demonstrated by means of simulations, as well as the pitfalls, when other phenomena like iron–boron pairing/dissociation, light- and elevated-temperature-induced degradation and regeneration, or surface-related degradation are superimposed. Finally, the concept of lifetime-equivalent defect density is extended to surface phenomena.**

***Index Terms*—Boron–oxygen-related light-induced degradation (BO-LID) and regeneration, crystalline silicon, defect density, defect dynamics, iron–boron (FeB) pair dissociation, light- and elevated-temperature-induced degradation (LeTID), surface-related degradation (SRD).**

I. Introduction

In many studies on degradation or, more generally, changes in bulk excess charge carrier lifetime, e.g., [1]–[12], these changes are quantified via a lifetime-equivalent defect density often also termed as effective, relative, or normalized defect density. Within this paper, the derivation and definition, as well as some general properties, of this quantity are reviewed. Its application to single-defect dynamics is illustrated by simulations in the context of boron–oxygen-related light-induced degradation (BO-LID), e.g., [2], [6], [13], [14]. Furthermore, typical pitfalls like superposition with the pairing/dissociation of iron–boron (FeB) pairs [15]–[19], light- and elevated-temperature-induced degradation (LeTID), e.g., [7]–[11], or surface-related degradation (SRD), e.g., [11], [12], [20], [21], are addressed. Finally, the definition of the lifetime-equivalent defect density is extended to surface phenomena.

Manuscript received March 14, 2019; revised May 4, 2019; accepted June 2, 2019. Date of publication June 27, 2019; date of current version August 22, 2019. This work was supported in part by the German Federal Ministry for Economic Affairs and Energy under Contract, 0324080C, 0325877C, and 0324204B.

The author is with the Department of Physics, University of Konstanz, 78457 Konstanz, Germany (e-mail: Axel.Herguth@uni-konstanz.de).

Color versions of one or more of the figures in this paper are available online at http://ieeexplore.ieee.org.

Digital Object Identifier 10.1109/JPHOTOV.2019.2922470

II. Basic Idea, Derivation, and Definition

In an experiment, it can be quite difficult to separate recombination via different mechanisms working in parallel. In general, the effective recombination rate $R_{\mathrm{eff}} = \Sigma_j R_j$ resulting from the superposition of individual rates R_j or, more commonly, the injection (Δn) and temperature-dependent effective excess charge carrier lifetime $\tau_{\mathrm{eff}} = \Delta n \,/\, R_{\mathrm{eff}}$ given by

$$\frac{1}{\tau_{\mathrm{eff}}} = \frac{1}{\tau_{\mathrm{surf}}} + \frac{1}{\tau_{\mathrm{intr}}} + \sum\nolimits_j \frac{1}{\tau_j} \tag{1}$$

is measured including a lifetime τ_{surf} related to surface recombination, a lifetime τ_{intr} related to intrinsic bulk recombination (comprising radiative and Auger-type mechanisms), and lifetimes τ_j related to various channels j of bulk recombination via defects. Especially, the latter ones can be numerous and, thus, hard to separate and assess properly. Even the description of intrinsic recombination is not that well defined as it may appear because it is quantified and parameterized—in all conscience—with the best samples available, exhibiting the least residual recombination aside from intrinsic recombination. Even though the mechanisms of intrinsic recombination of course do not change over time, the parameterization does every now and then [22]–[26].

However, in many studies, the focus lies on what changes due to a certain procedure, meaning effective lifetime changes from $\tau_{\mathrm{eff},B}$ *before* (B) to $\tau_{\mathrm{eff},A}$ *after* (A) the procedure. Thus, the difference in the inverse effective lifetime is of interest

$$\frac{1}{\tau_{\mathrm{eff},A}} - \frac{1}{\tau_{\mathrm{eff},B}} = \left[\frac{1}{\tau_{\mathrm{surf},A}} - \frac{1}{\tau_{\mathrm{surf},B}}\right] + \sum\nolimits_j \left[\frac{1}{\tau_{j,A}} - \frac{1}{\tau_{j,B}}\right]. \tag{2}$$

The first advantage is immediately obvious: Intrinsic recombination cancels out. For the time being, the surface-limited lifetime shall not change due to the procedure, meaning $\tau_{\mathrm{surf},A} = \tau_{\mathrm{surf},B}$, and only one bulk-related recombination channel x shall change. Then, the difference of inverse lifetimes (2) simplifies to

$$\frac{1}{\Delta\tau_{\mathrm{def}}} := \frac{1}{\tau_{\mathrm{eff},A}} - \frac{1}{\tau_{\mathrm{eff},B}} = \frac{1}{\tau_{x,A}} - \frac{1}{\tau_{x,B}} \tag{3}$$

isolating the change in influence of that recombination channel. It is, therefore, reasonable to define a defect-related lifetime change $\Delta\tau_{\mathrm{def}}$ from this difference of inverse lifetimes.

Typically, bulk recombination channels are related to specific defects and can be described by Shockley, Read, and Hall's (SRH) theory of recombination via isolated point-like defects, where recombination occurs via a single energy level E_t in the

otherwise forbidden band gap [27], [28]. However, it is noteworthy that this is not always the case, e.g., for extended defects like grain boundaries or extended clusters. The lifetime τ_{SRH} correlated with a single-level SRH defect is given by

$$\tau_{\mathrm{SRH}} = \frac{\tau_n\left(p_0 + p_1 + \Delta n\right) + \tau_p\left(n_0 + n_1 + \Delta n\right)}{p_0 + n_0 + \Delta n} \tag{4}$$

with p_0 and n_0 denoting the equilibrium densities of electrons and holes (in darkness), Δn the excess charge carrier density (injection), and p_1 and n_1 the respective densities at the defect

$$p_1 = N_v \cdot \exp\left(-\frac{E_t - E_v}{kT}\right) \text{ and } n_1 = N_c \cdot \exp\left(-\frac{E_c - E_t}{kT}\right) \tag{5}$$

depending on the "depth" of the defect energy level E_t in the forbidden band gap with respect to valence band edge E_v or conduction band edge E_c compared with mean thermal energy kT. The lifetimes τ_p and τ_n correspond to kinetic capture time constants of holes and electrons, respectively, defined as

$$\tau_p^{-1} = \sigma_p v_{\mathrm{th},p} \cdot N_{\mathrm{SRH}} \text{ and } \tau_n^{-1} = \sigma_n v_{\mathrm{th},n} \cdot N_{\mathrm{SRH}} \tag{6}$$

depending on capture cross sections σ_p and σ_n for holes and electrons, their thermal velocities $v_{\mathrm{th},p}$ and $v_{\mathrm{th},}n$, and, finally, on the density N_{SRH} of these defects. Thus, N_{SRH} can be factored out of (4)

$$\tau_{\mathrm{SRH}} = f \cdot N_{\mathrm{SRH}}^{-1} \tag{7}$$

with the prefactor f

$$f\left(\Delta n, T; p_0, n_0, \sigma_p, \sigma_n, E_t\right) = \frac{\frac{p_0 + p_1 + \Delta n}{\sigma_n v_{\mathrm{th},n}} + \frac{n_0 + n_1 + \Delta n}{\sigma_p v_{\mathrm{th},p}}}{p_0 + n_0 + \Delta n} \tag{8}$$

now carrying the dependence on injection Δn and absolute temperature T, both being directly accessible during the lifetime measurement. It, furthermore, accounts for material properties like equilibrium concentration p_0 and n_0 (given in most cases by the doping density of acceptors or donors), as well as for defect specific properties (σ_p, σ_n, and E_t).

For a "deep" energy level E_t (meaning $E_t - E_v \gg kT$ and $E_c - E_t \gg kT$), the SRH densities p_1 and n_1 are negligible with respect to the equilibrium densities p_0 or n_0 (depending on doping type) and/or the injection Δn. For p-type material ($n_0 = n_i^2/p_0 \ll p_0$ with n_i being the intrinsic charge carrier density), (4) may then be simplified to

$$\tau_{\mathrm{SRH}}^{*} = \tau_n \cdot \left(1 + \frac{\tau_p}{\tau_n} \cdot \frac{\Delta n}{p_0 + \Delta n}\right) \tag{9}$$

corresponding to the approach of Murphy *et al.* [29]. Factoring out N_{SRH} from (9) yields in this case the prefactor f^* as

$$f^*\left(\Delta n, T; p_o\right) = \frac{1}{\sigma_n v_{\mathrm{th},n}} \cdot \left(1 + \frac{\tau_p}{\tau_n} \cdot \frac{1}{1 + \frac{p_0}{\Delta n}}\right) \tag{10}$$

which depends rather on the ratio of injection Δn and doping density p_0 than on Δn and p_0 independently. For n-type material, an analogous approach is valid.

Inserting (7) into (3) yields

$$\frac{1}{\Delta\tau_{\mathrm{def}}} = \frac{1}{\tau_{\mathrm{eff},A}} - \frac{1}{\tau_{eff,B}} = \frac{1}{f} \cdot \left(N_{\mathrm{SRH},A} - N_{\mathrm{SRH},B}\right) = \frac{1}{f} \cdot \Delta N_{\mathrm{SRH}}. \tag{11}$$

As the difference of inverse lifetimes $\tau_{\mathrm{eff},B}$ before and $\tau_{\mathrm{eff},A}$ after the procedure is directly proportional to the change in defect density ΔN_{SRH}, it is a quantitative measure of ΔN_{SRH} directly accessible in an experiment even with no detailed knowledge of the prefactor f. It is, therefore, reasonable to define this difference of inverse lifetimes as a "lifetime-equivalent defect density" ΔN_{leq}

$$\Delta N_{\mathrm{leq}} := \frac{1}{\Delta\tau_{\mathrm{def}}} = \frac{1}{\tau_{\mathrm{eff},A}} - \frac{1}{\tau_{\mathrm{eff},B}} \quad \propto \Delta N_{\mathrm{SRH}}. \tag{12}$$

Note that ΔN_{leq} is only reasonable for differences of inverse lifetimes, but not for the inverse lifetime (1) itself because it would include terms not related to a scalable defect density. Also note that the unit of ΔN_{leq} is [s^{-1}].

There are alternative denominations of ΔN_{leq} used by various authors. For example, the terminologies "effective defect density," "relative defect density," or "normalized defect density" are encountered in the literature. It may be a question of taste which terminology is used; however, there is the risk of being deceptive. The terminology "defect density" implies at first glance a number of defects in a certain space volume, thus in units of [cm^{-3}], and irritation might be alleviated by speaking rather of a "lifetime-equivalent defect density." Furthermore, the terminology "normalized" typically means that a quantity is compared by its ratio to a certain value, and normalization then results in a dimensionless quantity.

III. Fundamental Properties

A. Injection and Doping Dependence

The lifetime-equivalent defect density ΔN_{leq} depends via the prefactor f (8) on temperature T, injection Δn, and doping density (p_0 or n_0) or, for a deep defect level, via f^* (10) rather on the ratio $\Delta n/p_0$ (or $\Delta n/n_0$). Hence, ΔN_{leq} may vary depending on the chosen T and Δn (or $\Delta n/p_0$) at which it is reported, even though ΔN_{SRH} has a fixed value. This is exemplarily illustrated in Fig. 1 for a deep mid-gap energy level with an asymmetric τ_p/τ_n ratio of 10. Within this simulation, intrinsic recombination was parameterized according to [26], and surface recombination was assumed to follow the J_0 model with $J_0 = 15$ fA/cm^2 (see Section VI). Depending on the injection, ΔN_{leq} varies from 20 to 2 ms^{-1} as the ratio $\tau_p/\tau_n = 10$ translates directly to f^* (10).

However, $\Delta N_{\mathrm{SRH}}(\Delta n)$ does not necessarily have to resemble a downward S-shape. For a "shallow" energy level, the situation can be completely inverted, as illustrated in Fig. 2. Shallow means in this context that E_t is that close to one of the band edges that either n_1 or p_1 (5) is no longer negligible. In this case, a shallow energy level above the valence band ($E_t = E_v + 0.1\,\mathrm{eV}$) was chosen together with a symmetric τ_p/τ_n ratio of 1. Again, intrinsic recombination was calculated according to [26], and

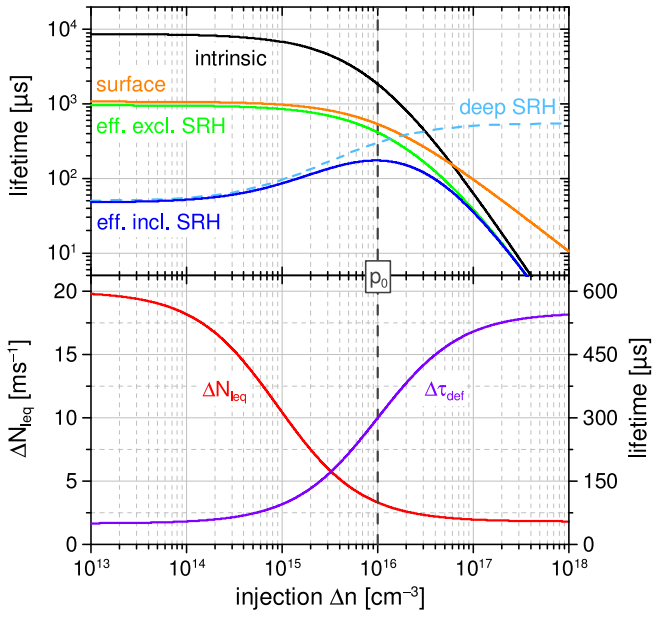

Fig. 1. (Top) Injection-dependent contribution of various recombination channels to the effective lifetime excluding (green solid line) and including (blue solid line) a single deep-level SRH defect (cyan dashed line). (Bottom) Injection-dependent lifetime-equivalent defect density ΔN_{leq} (red line) and defect lifetime $\Delta\tau_{\mathrm{def}}$ (violet line), the latter resembling the cyan dashed deep SRH curve. Calculations were done at $T = 300$ K and $p_0 = 10^{16}$ cm^{-3}.

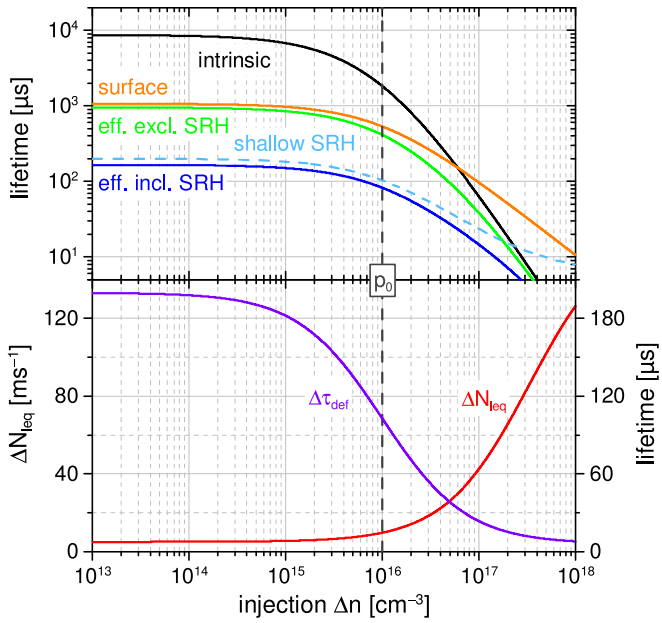

Fig. 2. (Top) Injection-dependent contribution of various recombination channels to the effective lifetime excluding (green solid line) and including (blue solid line) a single shallow SRH defect (cyan dashed line). (Bottom) Injection-dependent lifetime-equivalent defect density ΔN_{leq} (red line) and defect lifetime $\Delta\tau_{\mathrm{def}}$ (violet line), the latter resembling the cyan dashed shallow SRH curve. Calculations were done at $T = 300$ K and $p_0 = 10^{16}$ cm^{-3}.

surface recombination was assumed to follow the J_0 model with $J_0 = 15$ fA/cm^2.

B. Temperature Dependence

The temperature dependence of $f(8)$ or $f^*(10)$ arises from two points [30]: 1) The thermal velocities $v_{\mathrm{th},p}$ and $v_{\mathrm{th},n}$ follow a $\sqrt{T}$ dependence; hence, τ_p and τ_n follow the inverse trend, at least when assuming an independence of the capture cross sections σ_p and σ_n from temperature. The τ_p/τ_n ratio should remain unchanged as the individual temperature dependencies cancel out; and 2) the SRH densities p_1 and n_1 (5) depend strongly on temperature; however, they only play a role for shallow energy levels E_t. The effect of changing temperature from 300 to 400 K (27 to 127 °C) is illustrated in Fig. 3 for a series of defects with varying "depth" E_t in the forbidden band gap, while maintaining $\tau_n = 50\,\mu$s and $\tau_p/\tau_n = 10$.

For a deep defect level $E_t = E_c - 500$ meV (bottom graph), there is hardly any temperature dependence of ΔN_{leq} due to the relatively small change of $v_{\mathrm{th},n}$ and $v_{\mathrm{th},p}$ by only a factor of $\sqrt{300/400} \sim 0.87$, and thus, the injection-independent shift of ΔN_{leq} between the red dashed 300 K line and the red solid 400 K line toward higher values is barely visible on the logarithmic scale. For "shallower" defect levels, the change in temperature results in an injection-dependent change of ΔN_{leq}. While ΔN_{leq} increased globally for $E_t = E_c - 500$ meV, it even begins to decrease for $E_t > E_c - 450$ meV in low injection Δn; the stronger, the shallower the defect gets. Note that there occurs a crossing of the red dashed 300 K and solid 400 K ΔN_{leq} lines at a certain injection depending on the exact "depth" of the defect level. Furthermore, the transition from a downward S-shaped ΔN_{leq} curve of a deep defect level to an upward S-shaped ΔN_{leq} curve of a shallow defect level occurs at different depth for different temperatures. Whereas $\Delta N_{\mathrm{leq}}(\Delta n)$ is almost flat at $E_t = E_c - 200$ meV for 300 K (dashed lines), it is almost flat at $E_t = E_c - 300$ meV for 400 K (solid lines). For defect levels in between, the defect changes from "rather deep" at 300 K to "rather shallow" at 400 K. Thus, it should be carefully considered whether it is reasonable to compare ΔN_{leq} extracted at different temperatures.

It is also worth noting that the dependence of lifetime on temperature and injection is the basis for temperature- and injection-dependent lifetime spectroscopy, as demonstrated, e.g., in [31]–[34].

IV. Application Example

The lifetime-equivalent defect density ΔN_{leq} is often used to compare the dynamic of defect formation over the course of time. One very common example is the light-induced degradation and subsequent regeneration of bulk lifetime due to the formation and neutralization of boron–oxygen-related defects (BO-LID), e.g., [2], [6], [13], [14]. It is well described by defect reactions within a three-state defect model comprising an "annealed" recombination-inactive defect state, a "degraded" recombination-active defect state, and a "regenerated" recombination-inactive state [13], [14]. The formation of active defects (density N) over the course of time t from their precursors and their subsequent neutralization by conversion into the

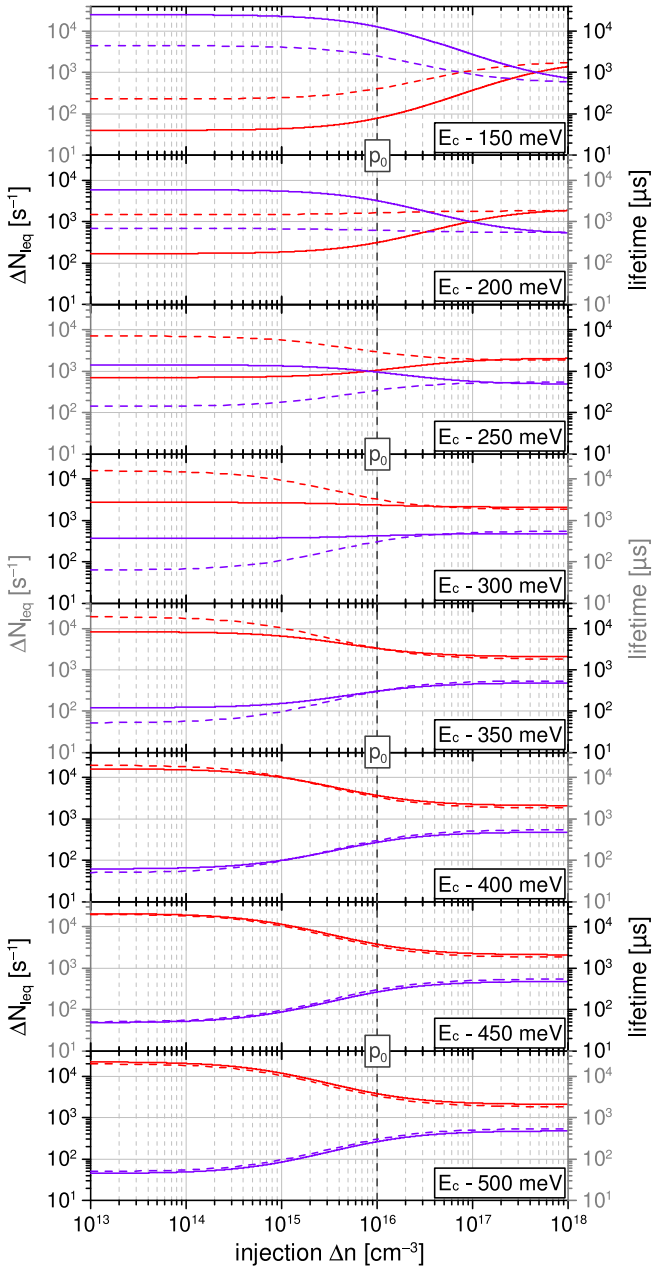

Fig. 3. Injection-dependent lifetime-equivalent defect density ΔN_{leq} (red) and defect lifetime $\Delta\tau_{\mathrm{def}}$ (violet) at 300 K (dashed lines) and 400 K (solid lines) with varying "depth" of the defect level. Calculations done at $p_0 = 10^{16}$ cm^{-3}.

regenerated state follows approximately

$$N(t) = -N_1 \cdot \exp\left(-\frac{t}{t_{\mathrm{deg}}}\right) + N_2 \cdot \exp\left(-\frac{t}{t_{\mathrm{reg}}}\right). \quad (13)$$

The prefactor N_1 determines the maximum density of defects that could form without regeneration. The prefactor N_2, or better the ratio N_2 / N_1, determines the completeness of regeneration. It should be noted that a complete regeneration ($N_2 = N_1$) does not necessarily have to occur [13], [35], [36]; however, in the following, a complete regeneration is assumed. The quantities t_{deg} and t_{reg} are characteristic time constants for degradation and regeneration [13]. For the sake of simplicity, the time constants

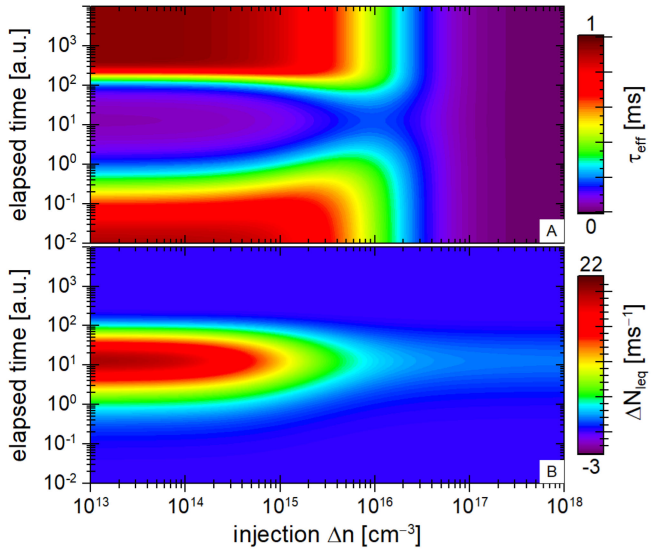

Fig. 4. Injection- and time-dependent evolution of effective lifetime τ_{eff} (a) and lifetime-equivalent defect density ΔN_{leq} (b) relative to $t = 0$ in a scenario that resembles BO-LID and subsequent regeneration thereof. Calculations were done at $T = 300$ K and $p_0 = 10^{16}$ cm^{-3}.

are chosen in the following rather arbitrarily to $t_{\mathrm{deg}} = 5$ [a.u.] (arbitrary time units) and $t_{\mathrm{reg}} = 10 \cdot t_{\mathrm{deg}}$ depicting a typical, but not mandatorily a specifically realistic scenario. Furthermore, again for the sake of simplicity, the recombination activity of the boron–oxygen-related defect is approximated by a single deep-level SRH defect with a τ_p/τ_n ratio of 10 (just as discussed in Fig. 1) [2], even though it is known that it actually features two energy levels and deviates slightly from the τ_p/τ_n ratio of 10 chosen here (see [6] and references therein for more details). Actual measurements may deviate in detail; however, the general setting remains valid.

Fig. 4 depicts the expected injection- and time-dependent evolution of the effective lifetime τ_{eff} [see Fig. 4(a)] and lifetime-equivalent defect density ΔN_{leq} [see Fig. 4(b)] choosing the same boundary conditions as in the context of Fig. 1. Even though lifetime drops significantly for higher injection Δn virtually independent of time due to dominant intrinsic recombination in the bulk, as well as recombination at the surface, ΔN_{leq} cancels this effect out and shows its highest values at low injection just as Fig. 1 illustrates.

Fig. 5 shows cutting lines at various injection levels marking the typically used injection range in lifetime measurements. Even though the maximum value of ΔN_{leq} depends on Δn, the shape is always similar as can be seen from the dashed ratio lines showing that the ratio of ΔN_{leq} at all injection levels relative to $\Delta n = 10^{16}$ cm^{-3} remains perfectly constant all the time.

V. Pitfalls

The lifetime-equivalent defect density ΔN_{leq} must be treated with caution in those cases, in which the assumptions within the derivation of ΔN_{leq} are not met. This is especially the case when not just one recombination channel changes but two or

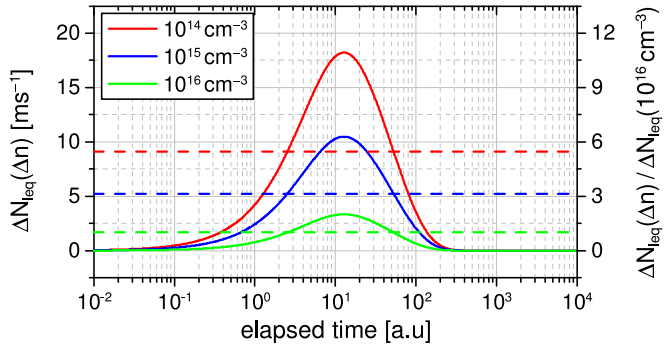

Fig. 5. Cutting lines of lifetime-equivalent defect density ΔN_{leq} (solid lines) at various injection levels Δn in Fig. 4. The dashed lines depict the ratio of ΔN_{leq} at various Δn relative to $\Delta n = 10^{16}$ cm^{-3}. Calculations were done at $T = 300$ K and $p_0 = 10^{16}$ cm^{-3}.

more. Then, ΔN_{leq} corresponds to the sum of changing individual defect densities ΔN_j weighed by their prefactor f_j or, in other words, their individual contributions $\Delta N_{\mathrm{leq},j}$

$$\Delta N_{\mathrm{leq}} = \frac{1}{\tau_{\mathrm{eff},A}} - \frac{1}{\tau_{\mathrm{eff},B}} = \sum\nolimits_j \left(\frac{1}{f_j} \cdot \Delta N_j \right) = \sum\nolimits_j \Delta N_{\mathrm{leq},j}. \tag{14}$$

Sections V-A to V-C depict different typical scenarios encountered in reality, where two different defect species are involved. One could easily construct even a superposition of all these scenarios. Section V-D discusses a very common pitfall encountered especially in laterally inhomogeneous multicrystalline material: comparing ΔN_{leq} of regions with different lifetime. Note that the scenarios are simulated with reasonable but not necessarily proven assumptions concerning the specific defect reaction kinetics.

A. Iron–Boron Pair Association and Dissociation

One very common contaminant in crystalline silicon is iron. Despite forming clusters and decorating grain boundaries, atomic iron prefers an interstitial site (Fe_i) and is preferentially positively charged. Due to its charge state, it repels holes and attracts electrons, which can be seen from the asymmetric capture cross sections $\sigma_p = 7 \times 10^{-17}$ cm^2 and $\sigma_n = 4 \times 10^{-14}$ cm^2 [18]. In the presence of boron and the absence of excess charge carriers, Fe_i prefers at low temperatures to form FeB pairs with the negatively charged acceptor boron. The matching of charges leads to more symmetric capture cross sections $\sigma_p = 5 \times 10^{-15}$ cm^2 and $\sigma_n = 3 \times 10^{-15}$ cm^2 [18]. However, in the presence of excess charge carriers or at elevated temperature (e.g., 200 °C), FeB pairs become instable and dissociate [15]–[18]. The effect of complete FeB pair dissociation on lifetime and lifetime-equivalent defect density is exemplarily illustrated in Fig. 6 for an iron contamination of $[\mathrm{Fe}_i]_A = [\mathrm{FeB}]_B = 5 \times 10^{10}$ cm^{-3} as often found in insufficiently gettered material. As the dissociation of FeB (e.g., by strong illumination) leads unavoidably to a concurrent decrease of [FeB] and increase of $[\mathrm{Fe}_i]$, the recombination activity of two defect species changes in parallel. The recombination via Fe_i and FeB features a peculiarity: There is a (doping-dependent) crossover point (cop) of the FeB

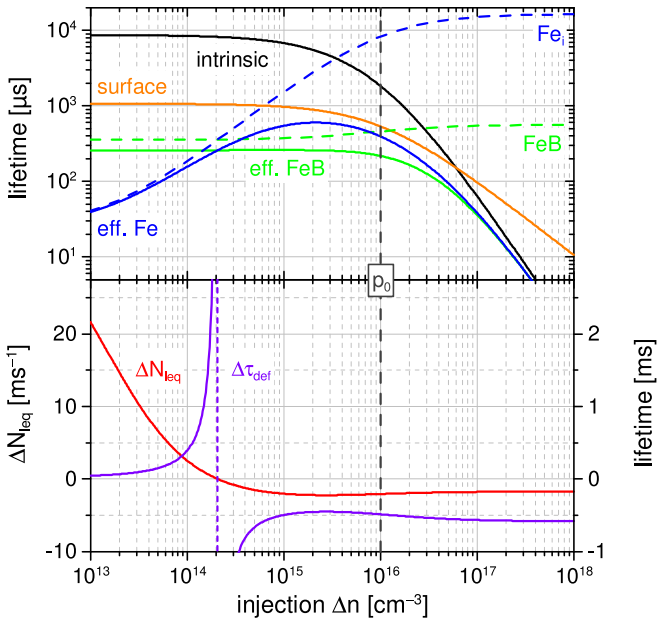

Fig. 6. (Top) Injection-dependent contribution of various recombination channels, especially FeB (green dashed line) and Fe_i (blue dashed line) to the effective lifetime including only FeB pairs (green solid line) and including only Fe_i (blue solid line). (Bottom) Injection-dependent lifetime-equivalent defect density ΔN_{leq} and defect lifetime $\Delta\tau_{\mathrm{def}}$ derived from the difference of inverse effective lifetimes. Calculations were done at $T = 300$ K and $p_0 = 10^{16}$ cm^{-3}.

and Fe_i lifetime curves ($\Delta n_{\mathrm{cop}} \sim 2 \times 10^{14}$ cm^{-3} in Fig. 6) implying that Fe_i (blue dashed line) is more harmful at injection levels below the crossover point than FeB (green dashed line) and less harmful at injection levels above the crossover point. This is also clearly visible in the derived lifetime-equivalent defect density

$$\Delta N_{\mathrm{leq}} = \frac{1}{\tau_{\mathrm{eff},A}} - \frac{1}{\tau_{\mathrm{eff},B}} = \left(\frac{1}{f_{\mathrm{Fe}}} - \frac{1}{f_{\mathrm{FeB}}} \right) \cdot [\mathrm{Fe}_i]_A \tag{15}$$

that changes its sign at the crossover point. Ignoring the injection-dependent prefactors f_{Fe} and f_{FeB} implies at first glance that more defects have formed at injection levels below the crossover point, and that defects have even vanished above the crossover point even though the total density of iron $[\mathrm{Fe}_i] + [\mathrm{FeB}]$ has not changed. It has only switched its state from FeB to Fe_i. Intentionally analyzing ΔN_{leq} at the crossover point will yield no change, and the correlated defect lifetime diverges.

B. Iron–Boron Pairs and Boron–Oxygen-Related Light-Induced Degradation Dynamics

A typical interference in investigations on light-induced degradation phenomena like BO-LID (see Section IV) is the unintentional superposition with FeB dissociation (see Section V-A) as light-induced degradation experiments often start after dark storage after which iron prefers the associated state FeB.

In the early phase, the FeB pairs dissociate with a comparably small time constant t_{Fe}, which is chosen in the following to 0.1 [a.u.]. The interstitial iron concentration $[\mathrm{Fe}_i]$ builds up, while the pair concentration [FeB] decays about exponentially from

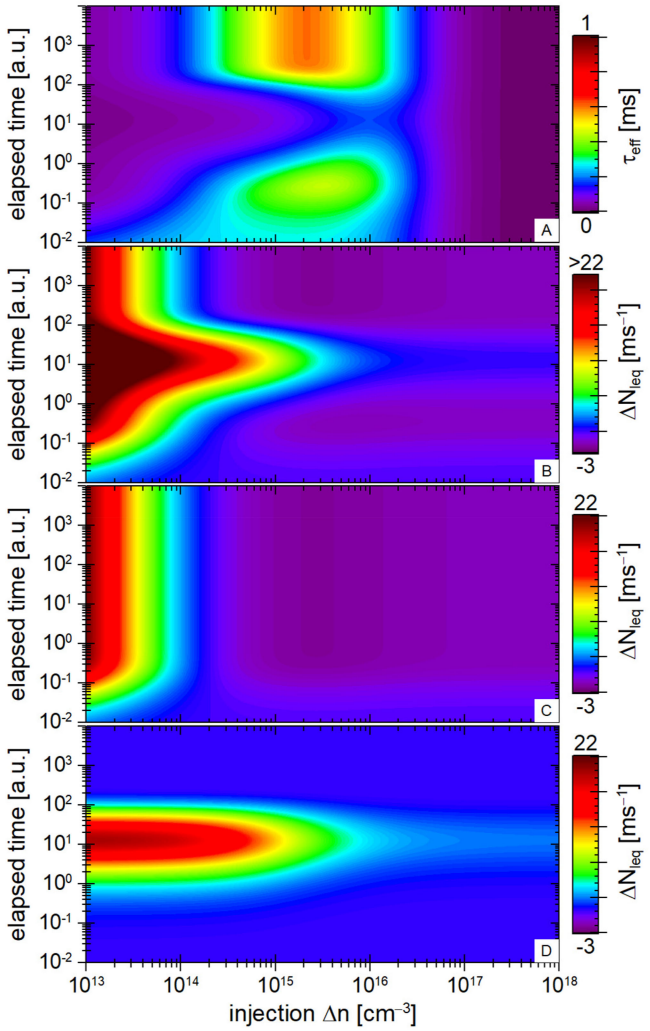

Fig. 7. Injection- and time-dependent evolution of effective lifetime τ_{eff} (a) and total lifetime-equivalent defect density ΔN_{leq} (b) relative to $t = 0$ in a scenario that resembles BO-LID and subsequent regeneration thereof superimposed by FeB pair dissociation in the early phase. (c) and (d) depict the individual defect contributions of the FeB/Fe$_i$ and BO-LID subsystem. Calculations were done at $T = 300$ K and $p_0 = 10^{16}$ cm^{-3}.

its initial value of $[\mathrm{FeB}]_{\max} = 5 \times 10^{10}$ cm^{-3}

$$\frac{[\mathrm{Fe}_i]\,(t)}{[\mathrm{FeB}]_{\max}} = 1 - \frac{[\mathrm{FeB}]\,(t)}{[\mathrm{FeB}]_{\max}} = 1 - \exp\left(-\frac{t}{t_{\mathrm{Fe}}}\right). \qquad (16)$$

Fig. 7 illustrates the temporal evolution of the superimposed FeB/Fe$_i$ and BO-LID defect subsystem assuming the same boundary conditions as in Section IV besides the addition of [FeB] and [Fe$_i$]. In contrast with the pure BO-LID scenario (see Fig. 4), τ_{eff} [see Fig. 7(a)] is now severely limited in low injection due to the presence of both FeB and Fe$_i$. The total lifetime-equivalent defect density ΔN_{leq} [see Fig. 7(b)] and the individual contributions $\Delta N_{\mathrm{leq,Fe}}$ and $\Delta N_{\mathrm{leq,BOLID}}$ of the FeB/Fe$_i$ [see Fig. 7(c)] and BO-LID [see Fig. 7(d)] subsystem are related to $t = 0$ or, in other words, related to the FeB state. As discussed before, the FeB pair dissociation results in negative $\Delta N_{\mathrm{leq,Fe}}$ values above the crossover point turning ΔN_{leq} negative as well, while increasing it below the crossover point.

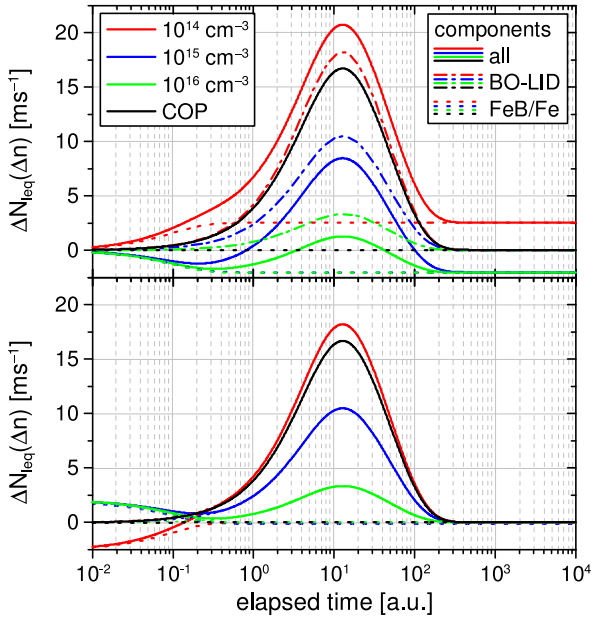

Fig. 8. (Top) Vertical cutting lines of lifetime-equivalent defect density ΔN_{leq} (solid lines) at various injection levels Δn and especially at the crossover point Δn_{cop} in Fig. 7(b). The dash-dotted lines depict the BO-LID component, and the dotted lines the FeB/Fe$_i$ component. (Bottom) Lifetime-equivalent defect density ΔN_{leq} at various injection levels Δn as in the top graph, but this time not related to $t = 0$, but $t = 10^4$. Calculations were done at $T = 300$ K and $p_0 = 10^{16}$ cm^{-3}.

Fig. 8 (top) depicts the evolution of ΔN_{leq} along cutting lines at various injection levels Δn (10^{14}, 10^{15}, and 10^{16} cm^{-3}) marking the typically used injection range in lifetime measurements and especially at $\Delta n_{\mathrm{cop}} \sim 2 \times 10^{14}$ cm^{-3}, which corresponds to the crossover point (cop) of the FeB and Fe$_i$ lifetime curves in Fig. 6. Depending on the injection level, the long-term value $\Delta N_{\mathrm{leq}}(\infty)$ is negative or positive except for Δn_{cop}. Ignoring the changes in the FeB/Fe$_i$ subsystem and simply using the double-exponential approach (13) to describe BO-LID requires $N_1 \neq N_2$ in (13) to fulfill $\Delta N_{\mathrm{leq}}(\infty) \neq 0$ (except for Δn_{cop}), even though $N_1 = N_2$ was assumed. Hence, one could erroneously conclude that regeneration is either incomplete ($\Delta N_{\mathrm{leq}}(\infty) > 0$; thus, $N_2 < N_1$) or even "more than complete" ($\Delta N_{\mathrm{leq}}(\infty) < 0$; thus, $N_2 > N_1$) depending on the injection level at which the analysis is done. However, even then, such an approach will not describe the distortion due to FeB dissociation in the early phase.

Calculating $\Delta N_{\mathrm{leq}}(t)$ relative to $t = 10^4$ [a.u.], or in other words relative to the Fe state, as shown in Fig. 8 (bottom), levels the curves in long term, thus solving the problem of apparent variable completeness of regeneration depending on the injection level, but, in this case, ΔN_{leq} turns negative or positive in the early phase. In principle, the best way to solve these issues (apart from removing Fe from the sample in the first place if possible) is to either carefully prepare the FeB/Fe$_i$ system to the same state for each measurement or to analyze $\Delta N_{\mathrm{leq}}(t)$ at the crossover point (cop, black lines in Fig. 8), where FeB dissociation plays no role at all, and $\Delta N_{\mathrm{leq}}(t)$ perfectly follows the double-exponential approach (13). The relevance of the FeB/Fe$_i$ for the interpretation of dynamics of the BO-LID subsystem and

how analyzing data at Δn_{cop} can help to minimize the influence of FeB/Fe_i was, e.g., demonstrated in [19].

C. Boron–Oxygen-Related Light-Induced Degradation and Light- and Elevated-Temperature-Induced Degradation

As of late, e.g., in [8]–[11], and [37], it is discussed that especially monocrystalline silicon grown by Czochralski's method (Cz-Si) suffers not only from BO-LID (due to its high oxygen contamination level), but from light- and temperature-induced degradation (LeTID) [7]–[11], [38]–[40] in parallel as well, which is attributed to the formation of an unknown defect species. Just like BO-LID, LeTID features a regeneration phase as well, and defect dynamic is, at least in the context of this paper, sufficiently well described by a time-dependent defect formation (13) similar to BO-LID. If BO-LID and LeTID occur in parallel, $\Delta N_{\mathrm{leq}}(t)$ corresponds to

$$\Delta N_{\mathrm{leq}}(t) = \frac{1}{f_{\mathrm{BOLID}}} \cdot N_{\mathrm{BOLID}}(t) + \frac{1}{f_{\mathrm{LeTID}}} \cdot N_{\mathrm{LeTID}}(t) \tag{17}$$

with $N_{\mathrm{BOLID}}(t)$ and $N_{\mathrm{LeTID}}(t)$ individually being described by (13) including the respective degradation and regeneration time constants t_{deg} and t_{reg} of both phenomena. Fig. 9 shows a simulation of the evolution of τ_{eff} [see Fig. 9(a)] and ΔN_{leq} [see Fig. 9(b)] related to $t = 0$ assuming $t_{\mathrm{deg,BOLID}} = 5$ [a.u.] and $t_{\mathrm{reg,BOLID}} = 10 \cdot t_{\mathrm{deg,BOLID}}$ (as used in Fig. 4). As LeTID seems to occur on a longer timescale and partially overlaps with BO-LID, the time constants were deliberately chosen to $t_{\mathrm{deg,LeTID}} = 50$ [a.u.] and $t_{\mathrm{reg,LeTID}} = 10 \cdot t_{\mathrm{deg,LeTID}}$. Furthermore, LeTID features a stronger injection dependence of lifetime than BO-LID, and the assumed $(\tau_p/\tau_n)_{\mathrm{LeTID}} = 30$ [9], [41] is noticeably larger than $(\tau_p/\tau_n)_{\mathrm{BOLID}} = 10$ (as used in Fig. 4). Moreover, LeTID is assumed to be less harmful in this example ($\tau_{n,\mathrm{LeTID}} = 75\ \mu$s) than BO-LID ($\tau_{n,\mathrm{BOLID}} = 50\ \mu$s).

At first glance, ΔN_{leq} in Fig. 9(b) and the $\Delta N_{\mathrm{leq}}(t)$ cutting lines along various injection levels Δn shown in Fig. 10 (solid lines) look somehow similar to ΔN_{leq} in Figs. 4 and 5, even though there is a delayed regeneration phase. One might overlook that there is a second defect system (dotted line) active besides the BO-LID subsystem (dash-dotted line) and simply conclude that $t_{\mathrm{reg,BOLID}}$ is, for whatever reason, higher than in Fig. 4. However, this impression vanishes if the ratio of $\Delta N_{\mathrm{leq}}(t)$ at various injection levels Δn relative to $\Delta N_{\mathrm{leq}}(t)$ at $\Delta n = 10^{16}$ cm^{-3} is taken into account (dashed lines). As BO-LID is assumed to occur earlier than LeTID, the ratio is dominated in the early phase by $(\tau_p/\tau_n)_{\mathrm{BOLID}}$, but dominated by $(\tau_p/\tau_n)_{\mathrm{LeTID}}$ in long term when LeTID becomes the dominant effect. Thus, it might be a good idea to not only analyze defect kinetics via $\Delta N_{\mathrm{leq}}(t)$ at just one injection level Δn, but also to benefit from injection-dependent information, maybe indicating the presence of more than one defect species.

D. Comparison of Different Lifetime Regions

A different pitfall may result from lateral inhomogeneity of lifetime samples, be it monocrystalline Cz-Si or FZ-Si (grown by

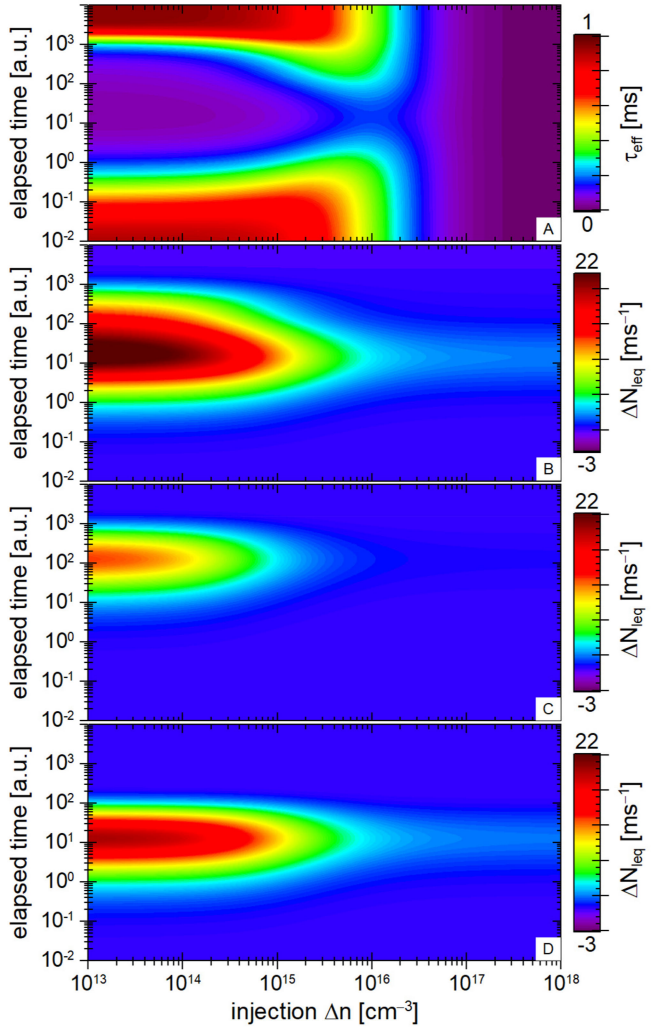

Fig. 9. Injection- and time-dependent evolution of effective lifetime τ_{eff} (a) and lifetime-equivalent defect density ΔN_{leq} (b) relative to $t = 0$ in a scenario that resembles BO-LID and subsequent regeneration thereof as well as LeTID and subsequent regeneration thereof. (c) and (d) separately depict the LeTID and BO-LID components of ΔN_{leq}. Calculations were done at $T = 300$ K and $p_0 = 10^{16}$ cm^{-3}.

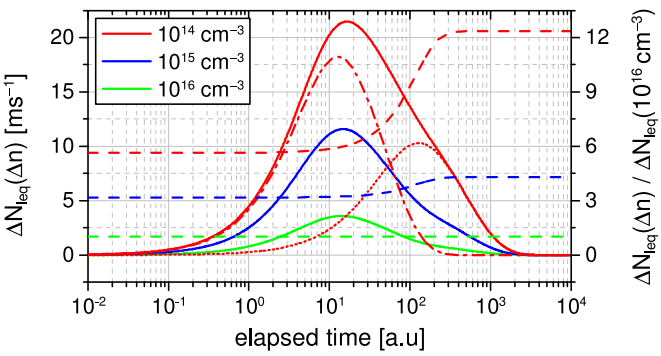

Fig. 10. Cutting lines (solid) of lifetime-equivalent defect density ΔN_{leq} at various injection levels Δn in Fig. 9(b). The dash-dotted and dotted lines exemplarily show the BO-LID and LeTID components for $\Delta n = 10^{14}$ cm^{-3}. The dashed lines depict the ratio of ΔN_{leq} at various Δn relative to $\Delta n = 10^{16}$ cm^{-3}. Calculations were done at $T = 300$ K and $p_0 = 10^{16}$ cm^{-3}.

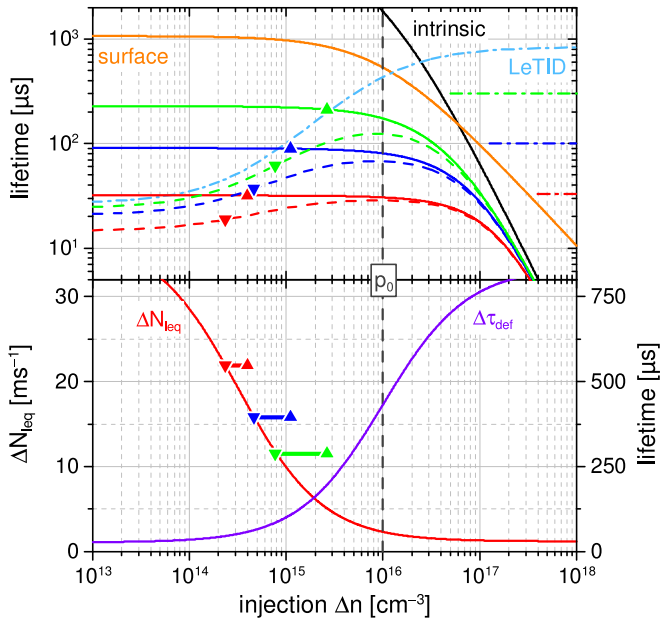

Fig. 11. (Top) Injection-dependent contribution of various recombination channels (intrinsic, surface, and LeTID) to the effective lifetime assuming different injection-independent background lifetimes of 33 μs (red), 100 μs (blue), and 300 μs (green) indicated as dash-dotted lines at high injection. Solid lines mark the effective lifetime excluding the LeTID component, whereas dashed lines correspond to effective lifetimes including the LeTID component. The upward and downward triangles correspond to the injection level and the corresponding effective lifetime obtained under constant generation conditions. (Bottom) Injection-dependent lifetime-equivalent defect density ΔN_{leq} (red line) and defect lifetime $\Delta\tau_{\mathrm{def}}$ (violet line) related to the LeTID component being the same for the different background lifetimes. The upward and downward triangles mark the values of ΔN_{leq} derived from the respective marked lifetime differences and the injection-level range in which it was derived. Calculations were done at $T = 300$ K and $p_0 = 10^{16}$ cm^{-3}.

the floating zone process) or multicrystalline silicon (mc-Si), due to variations in surface passivation quality and background bulk lifetime in combination with lifetime measurement techniques, which determine an effective lifetime not at a certain injection level Δn, but at a certain constant generation G. For example, this is often the case when photoluminescence imaging (PLI) techniques are used, where the luminescence intensity ϕ (being in p-type material proportional to $(p_0 + \Delta n) \cdot \Delta n$ or $p_0 \cdot \Delta n$ for $\Delta n \ll p_0$) is used as a measure of effective lifetime τ_{eff} according to the low-injection steady-state condition

$$G \cdot \tau_{\mathrm{eff}} = \Delta n \propto \phi. \tag{18}$$

Consider, for example, the following scenario: three grains of a mc-Si sample feature different injection-independent background lifetimes of 33 μs (red), 100 μs (blue), and 300 μs (green). In addition to these background limitations, LeTID occurs as well with the same defect density in all regions limiting the LeTID-related lifetime component τ_{LeTID} after degradation to 100 μs at $\Delta n = 10^{15}$ cm^{-3} (being one-tenth of $p_0 = 10^{16}$ cm^{-3}). Fig. 11 (top) shows the injection-dependent lifetime curves $\tau_{\mathrm{eff}}(\Delta n)$ in the different regions before (solid lines) and after occurrence of LeTID (dashed lines). During lifetime assessment by PLI, a constant generation rate $G = 1.25 \times 10^{19}$ cm$^{-3}\cdot$s^{-1} (corresponding approximately to one sun illumination [42]) is used, meaning that a certain combination of Δn and τ_{eff} is reached according to (18) for the different $\tau_{\mathrm{eff}}(\Delta n)$ curves, which is marked by the upward (prior to degradation) and downward triangles (after degradation). The first thing to note is that not only τ_{eff} varies due to degradation as expected, but Δn deviates as well, which additionally enlarges the loss in τ_{eff} already present at constant injection. Now, ignoring that discrepancy in injection level (due to lack of truly injection-dependent τ_{eff} data), one could calculate ΔN_{leq} according to its definition (12) with the τ_{eff} values from the three grains before and after degradation, as shown in Fig. 11 (bottom). The fully injection-dependent $\Delta N_{\mathrm{leq}}(\Delta n)$ curve (red line), which is—by definition—the same in the three different grains, is depicted as well. Obviously, the ΔN_{leq} values (red, blue, and green) calculated with (12) differ by a factor of 2, even though the assumed extent of LeTID is identical in all grains. Hence, the seemingly obvious explanation of LeTID affecting the three grains differently is a misinterpretation caused by the neglected/unknown injection dependence. A comparably easy-to-implement countermeasure to avoid that misinterpretation could be to combine measurements done at various generation rates or to adapt the generation rate G individually for each grain so that each grain features a similar luminescence flux (and injection level). Such an approach was, e.g., proposed by Heinz *et al.* [43].

With regard to the properties of the FeB/Fe$_i$ defect system discussed in Section V-A, one can easily construct another interesting example showing the pitfalls in laterally inhomogeneous systems. Consider two grains in mc-Si with same iron contamination but different constant background lifetimes so that injection $\Delta n_1 < \Delta n_{\mathrm{cop}}$ in the first grain and injection $\Delta n_2 > \Delta n_{\mathrm{cop}}$ in the second grain. According to Fig. 6, a similar dissociation of FeB to Fe$_i$ results in apparently positive $\Delta N_{\mathrm{leq},1}$ values in the first grain and apparently negative $\Delta N_{\mathrm{leq},2}$ values in the second grain. Hence, ignoring the different injection levels, one could conclude that defects have formed in the first grain and vanished in the second grain, even though the dissociation of FeB to Fe$_i$ is similar, and the total iron contamination has not changed at all. To escalate the situation even more, one should note that iron is typically far from homogeneously distributed in mc-Si, as shown, e.g., in [44] and [45], and thus, the injection-related apparent ΔN_{leq} variation mixes with actual [Fe] variation.

VI. Extension to Surfaces

A. Basic Idea, Derivation, and Definition

During the derivation of ΔN_{leq}, it was assumed that the surface-related lifetime τ_{surf} does not change. However, this assumption is not always valid in experiments, e.g., [11], [12], [20], [21]. In the following, it will be shown that the definition of ΔN_{leq} can be extended to surface phenomena as well, even though the meaning of "what a defect is" might change. In the above simulations, surface recombination was parameterized using a J_0 model stating for p-type material that

$$\frac{1}{\tau_{\mathrm{surf}}} = \frac{2\,(p_0 + \Delta n)}{qwn_i^2} \cdot J_0 \tag{19}$$

with q being the elementary charge, w the sample thickness, and n_i the intrinsic charge carrier density.

The injection dependence of a surface-related lifetime following the J_0 model differs fundamentally from that of a deep SRH bulk defect, as can be seen in Fig. 1. In contrast with the increasing lifetime with increasing injection related to a deep SRH bulk defect, surface-related lifetime decreases with increasing injection, and this allows, in principle, for a separation of recombination via a deep SRH bulk defect and J_0-like surface recombination [46]. In fact, the saturating or constant injection dependence of deep SRH bulk defects toward high injection is the basis for the determination of emitter saturation current densities (J_{0e}) on lowly doped substrates [47], [48]. If, e.g., material doped to $p_0 \sim 10^{14}$ cm^{-3} is used, the lifetime related to a deep SRH bulk defect almost saturates in the injection range of $\Delta n > 10^{16}$ cm^{-3} typically used for J_{0e} evaluation. However, determining J_0 using higher doped material (e.g., doped with $p_0 \sim 10^{16}$ cm^{-3}) is not that straightforward anymore because the upward bending of the SRH lifetime curve compensates at least in parts the downward bending of the surface-related lifetime curve and results in an apparent correlation of J_0 and τ_{SRH} [11]. The situation becomes even worse when it comes to the superposition of a shallow SRH bulk defect with a J_0-like surface, as shown in Fig. 2. Even though there is a different behavior in high injection (meaning $\Delta n \gg p_0$), τ_{SRH} and τ_{surf} behave similar for moderate and low injection ($\Delta n \leq 10^{16}$ cm^{-3}) typically accessible in experiments.

Besides emitter structures, the J_0 model works well for surface passivation layers carrying a high fixed charge density Q (like silicon nitride and aluminum oxide often used in LID studies) [49] because the fixed charges induce a band bending similar to that caused by an emitter rendering the surface saturation current density J_0 (related to one sample surface) injection independent. Hence, a changing surface-related lifetime τ_{surf} corresponds to a change in J_0

$$\frac{1}{\tau_{\mathrm{surf},A}} - \frac{1}{\tau_{\mathrm{surf},B}} = \frac{2\,(p_0 + \Delta n)}{qwn_i^2} \cdot (J_{0,A} - J_{0,B}) \propto \Delta J_0 \tag{20}$$

As shown by McIntosh and Black [49], J_0 may be expressed in terms of surface recombination velocity and fixed charge density (in the case of high Q)

$$J_0 = 2qkT\varepsilon_{Si} n_i^2 \cdot \frac{S_{\mathrm{mcc}}}{Q^2} = 2qkT\varepsilon_{Si} n_i^2 \cdot \frac{\sum_j S_{\mathrm{mcc},j}}{Q^2} \tag{21}$$

with ε_{Si} being the permittivity of silicon and S_{mcc} the total surface recombination velocity of minority charge carriers (mcc) at the surface. In analogy to bulk recombination, $S_{\mathrm{mcc}} = \Sigma_j\, S_{\mathrm{mcc}j}$ typically comprises various different defect species j each contributing in parallel with their specific $S_{\mathrm{mcc},j}$. The individual recombination velocities $S_{\mathrm{mcc},j}$ correspond to

$$S_p = \sigma_p v_{\mathrm{th},p} \cdot N_{\mathrm{SRH}} \text{ or } S_n = \sigma_n v_{\mathrm{th},n} \cdot N_{\mathrm{SRH}} \tag{22}$$

of either holes or electrons depending on which species is the minority charge carrier species at the surface. S_p and S_n are used equivalently to τ_p and τ_n (6) when describing surface recombination by the SRH formalism adapted to surfaces. However, in contrast with the typical situation encountered in the bulk, where injection Δn comes close to doping p_0 or n_0 and τ_{SRH} is noticeably injection dependent, the surface is in the case of high charge densities Q either in accumulation or inversion resembling low-injection conditions for the minority carrier species at the surface, and hence, capture of minority carriers is recombination limiting. In the case of surface (interface) defects, N_{SRH} is in units of [cm^{-2}].

If only one surface defect species x changes, combining (20) and (21) yields

$$\frac{1}{\tau_{\mathrm{surf},A}} - \frac{1}{\tau_{\mathrm{surf},B}} = \frac{4\varepsilon_{Si} kT\,(p_0 + \Delta n)}{w} \cdot \left(\frac{S_{\mathrm{mcc},x,A}}{Q_A^2} - \frac{S_{\mathrm{mcc},x,B}}{Q_B^2}\right) \tag{23}$$

and, as $S_{\mathrm{mcc},x}$ is proportional to $N_{\mathrm{SRH},x}$ (22), it seems reasonable to define ΔN_{leq} at the surface as

$$\Delta N_{\mathrm{leq}} := \frac{1}{\tau_{\mathrm{surf},A}} - \frac{1}{\tau_{\mathrm{surf},B}} = f_s \cdot \left(\frac{N_{\mathrm{SRH},x,A}}{Q_A^2} - \frac{N_{\mathrm{SRH},x,B}}{Q_B^2}\right) \tag{24}$$

in analogy to the bulk scenario with the prefactor f_s

$$f_s\,(\Delta n, T; p_0, \sigma_{\mathrm{mcc},x}) = \frac{4\ kT\varepsilon_{Si}\ \sigma_{\mathrm{mcc},x} v_{\mathrm{th,mcc}}}{w} \cdot (p_0 + \Delta n) \tag{25}$$

carrying the doping and injection dependence. Even though f_s comprises the specific capture cross section $\sigma_{\mathrm{mcc},x}$, the injection dependence of f_s is, in contrast with f (8) and f^* (10) in the bulk scenario, rather unspecific as it does only comprise minority, but not majority carrier information. Hence, f_s does not allow for defect identification.

Note that in the case of changes in surface passivation quality, two types of "defects" may be responsible. On the one hand, there can be recombination active defects at the interface that degrade the chemical passivation, which are represented by a change $\Delta N_{\mathrm{SRH}} = N_{\mathrm{SRH},A} - N_{\mathrm{SRH},B}$ in (24), and if fixed charge density does not change ($Q_A = Q_B$), ΔN_{leq} is directly proportional to ΔN_{SRH} just as it is in the bulk scenario. However, there can be a second kind of "defect" related to the formation or annihilation of a fixed charge density ΔQ within the passivation layer (or on the surface, e.g., by corona charging), which does not directly result in changing recombination activity at these "charge carrying defects," but rather indirectly results in changing recombination activity at already existing defects at the dielectric/silicon interface. Both phenomena may occur in parallel as discussed, e.g., in [11].

Whether one or the other mechanism is responsible for an observed change plays a role for the transfer function of ΔN_{SRH} or ΔQ to ΔN_{leq}, which can be illustrated with the following example. Assume that $\Delta N_{\mathrm{SRH}}(t)$ and $\Delta Q(t)$ show an exponentially saturating change ($X = N_{\mathrm{SRH}}$, Q)

$$\Delta X\,(t) = (\Delta X_A - \Delta X_B) \cdot \left[1 - \exp\left(-\frac{t}{t_X}\right)\right] \tag{26}$$

with t_X being a characteristic time constant. Fig. 12 illustrates how $\Delta N_{\mathrm{SRH}}(t)$ (red line) and $\Delta Q(t)$ (blue and green line) translate to $\Delta N_{\mathrm{leq}}(t)$ when only one mechanism is active. As ΔN_{leq} is

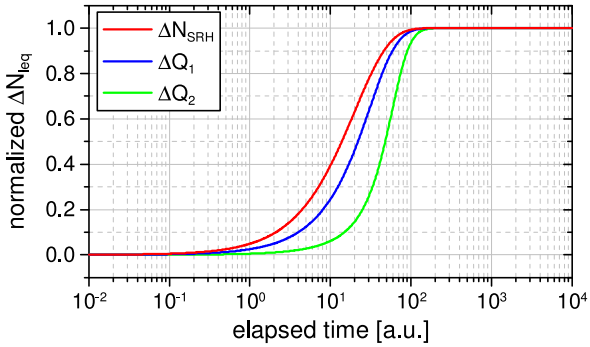

Fig. 12. Time-dependent evolution of ΔN_{leq} normalized to $\Delta N_{\mathrm{leq}}(\infty)$ in the case of changing surface defect density N_{SRH} and changing fixed charge density Q.

directly proportional to ΔN_{SRH}, $\Delta N_{\mathrm{leq}}(t)$ (red line) corresponds directly to the exponentially saturating curve of $\Delta N_{\mathrm{SRH}}(t)$. For the transfer function of $\Delta Q(t)$ to $\Delta N_{\mathrm{leq}}(t)$, the absolute values *before* (Q_B) and *after* degradation (Q_A) play a role. In a first scenario, $Q_B = 10 \times 10^{11}$ q/cm^2 (with Q being defined as multiple of the elementary charge q) decays to $Q_{A,1} = 5 \times 10^{11}$ q/cm^2 (blue line) and in a second scenario to $Q_{A,2} = 1 \times 10^{11}$ q/cm^2 (green line). As can be seen in Fig. 12, the exact value of Q_A has an impact on the exact shape of $\Delta N_{\mathrm{leq}}(t)$, and it does not resemble the assumed exponentially saturating shape of $\Delta Q(t)$ that is given by red $\Delta N_{\mathrm{SRH}}(t)$ line.

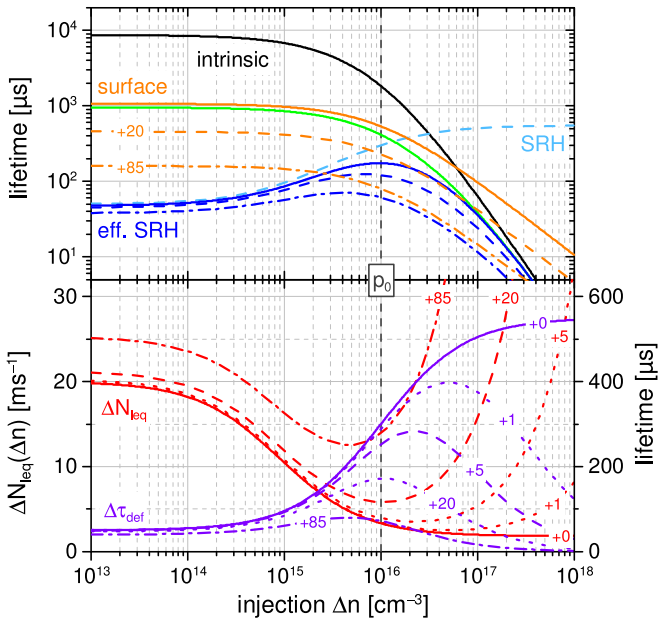

Fig. 13. (Top) Injection-dependent contribution of various recombination channels to the effective lifetime excluding (green solid line) and including (blue solid line) a single deep-level SRH defect (dashed cyan line). The dashed and dash-dotted orange lines depict a change in surface passivation quantified by a change in J_0 (in fA/cm^2) and how it changes the effective lifetime (dashed and dash-dotted blue line). (Bottom) Injection-dependent lifetime-equivalent defect density ΔN_{leq} and defect lifetime $\Delta\tau_{\mathrm{def}}$ derived from the difference of inverse effective lifetimes (green and blue curves). The red/violet numbers quantify the change in J_0 (in fA/cm^2) in addition to the occurrence of the deep-level SRH defect. Calculations were done at $T = 300$ K and $p_0 = 10^{16}$ cm^{-3}.

B. Instable Surface Passivation

Instable surface passivation can superimpose changes occurring in the bulk, as illustrated in Fig. 13, which is based on ΔN_{leq} of a deep-level SRH defect shown in Fig. 1. However, in addition to the occurrence of the bulk defect, a deterioration of surface lifetime (orange line) in terms of a change in J_0 (indicated as added values) from initially 15 fA/cm^2 is depicted. Whether the change in J_0 originates from a change in N_{SRH} or Q is meaningless here. As the prefactor f_s (25) comprises the term $(p_0 + \Delta n)$, small changes of J_0 (+1 fA/cm^2) show up first in ΔN_{leq} in high injection, where $\Delta n \gg p_0$, but then creep toward the lower injection regime for stronger changes of J_0 (+5 fA/cm^2), while becoming disastrous in high injection. For even stronger deterioration of J_0 (+20 fA/cm^2 and more), ΔN_{leq} begins to shift upward with $p_0 \cdot \Delta J_0$.

In many cases, injection-dependent lifetime data are only available up to $\Delta n \sim 1 \times 10^{16}$ cm^{-3}, and the strong increase of ΔN_{leq} in high injection is not observable. For moderate changes of J_0 (like +20 fA/cm^2), ΔN_{leq} is shifted upward and slightly deformed toward the upper limit $\Delta n \sim 1 \times 10^{16}$ cm^{-3} of available data, which could be erroneously interpreted as fingerprint of a less asymmetric deep SRH defect. For example, the ΔN_{leq} line with +20 fA/cm^2 looks rather like a deep bulk defect with $\tau_p/\tau_n \sim 6$, even though the actual defect features $\tau_p/\tau_n = 10$. Hence, it is important to take the possibility of surface passivation instability into account when the concept of ΔN_{leq} is used for the evaluation of changes in the bulk.

C. Surface-Related Degradation Superimposed to Boron–Oxygen-Related Light-Induced Degradation

An often encountered issue in the context of bulk-related LID studies is an unwanted dynamic instability of surface passivation quality. Such a situation is depicted in Figs. 14 and 15. The base scenario is the same BO-LID scenario as in Fig. 4 with $t_{\mathrm{deg}} = 5$ [a.u.] and $t_{\mathrm{reg}} = 10 \cdot t_{\mathrm{deg}}$. In addition, SRD [11], [12], [20], [21] is assumed to occur single exponentially saturating with J_0 rising from 15 to 100 fA/cm^2 with a time constant $t_{\mathrm{SRD}} = 500$ [a.u.]. A regeneration phase of SRD, as observed in [11] and [21], is ignored here. As can be seen from Fig. 14(b) and (c), SRD kicks-in at high injection levels Δn already at $t < 10$ [a.u.] and, thus, well before t_{SRD} due to the high sensitivity of f_s (25) in high injection. Only at low and moderate injection levels $\Delta n \ll p_0$, SRD occurs as expected on the time scale of t_{SRD}. Nevertheless, SRD overlaps with BO-LID and prevents a complete recovery of τ_{eff} and ΔN_{leq} from BO-LID before SRD sets in, even though the time scale of the recovery from BO-LID is by an order of magnitude shorter than that of SRD.

This can also be seen from the cutting lines in Fig. 15, where ΔN_{leq} features an intermediate minimum in between the recovery from BO-LID and the onset of SRD. However, the position and extent of this minimum depends on the chosen injection level because the individual ΔN_{leq} components of BO-LID and SRD feature an inverse trend. Whereas the extent of BO-LID decreases with injection, the extent of SRD increases with injection. This results in a flipped line order with, e.g., the black

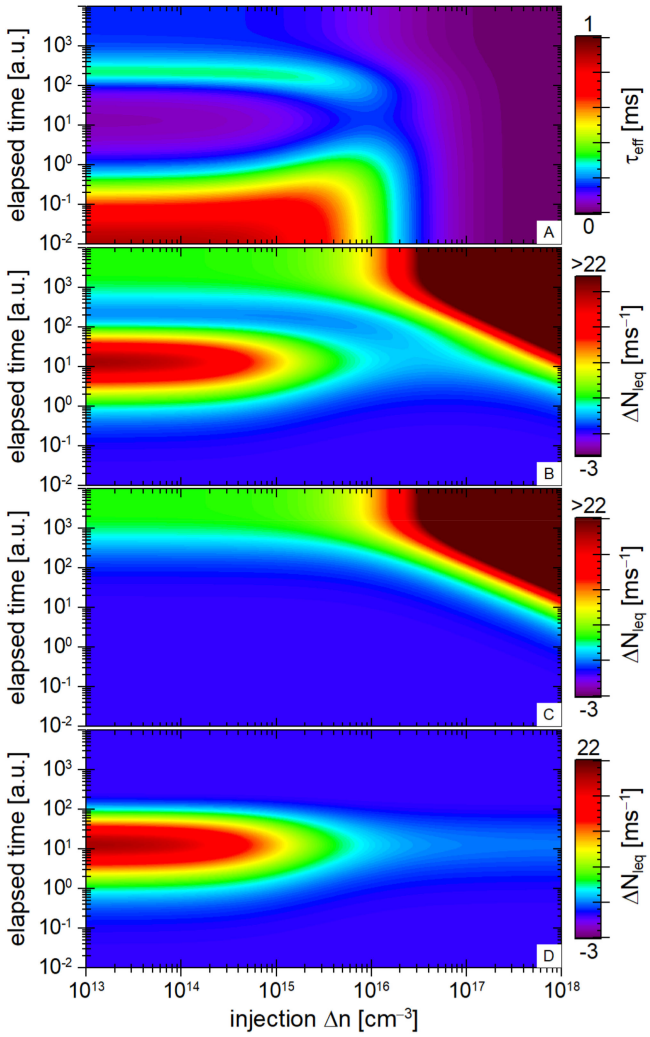

Fig. 14. Injection- and time-dependent evolution of effective lifetime τ_{eff} (a) and lifetime-equivalent defect density ΔN_{leq} (b) relative to $t = 0$ in a scenario that resembles BO-LID and subsequent regeneration thereof as well as SRD. (c) and (d) separately depict the SRD and BO-LID components of ΔN_{leq}. Note that the ΔN_{leq} scale was intentionally limited to 22 ms^{-1}, even though the SRD component exceeds this value by far in high injection. Calculations were done at $T = 300$ K and $p_0 = 10^{16}$ cm^{-3}.

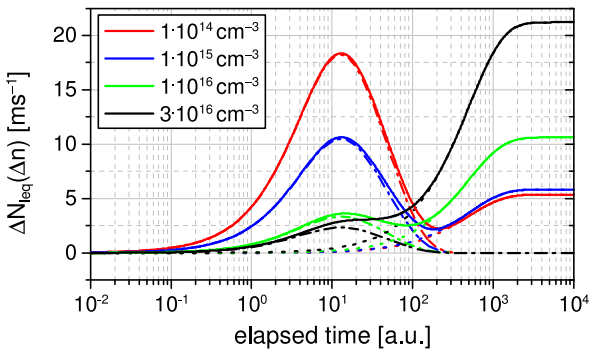

Fig. 15. Cutting lines (solid) of lifetime-equivalent defect density ΔN_{leq} at various injection levels Δn in Fig. 14(b). The dash-dotted and dotted lines show the respective SRD and BO-LID components from Fig. 14(c) and (d). Calculations were done at $T = 300$ K and $p_0 = 10^{16}$ cm^{-3}.

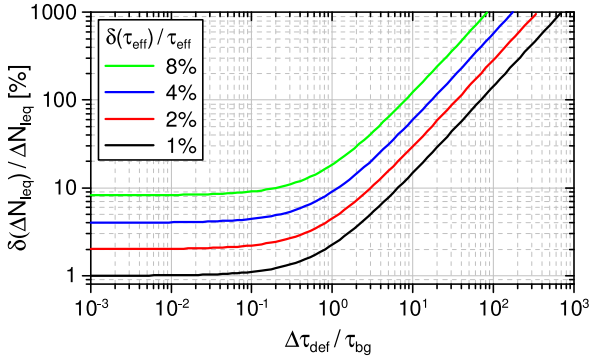

Fig. 16. Relative uncertainty of ΔN_{leq} in dependence of the ratio of defect-related lifetime $\Delta\tau_{\mathrm{def}}$ and background lifetime τ_{bg} for various relative uncertainties of the effective lifetime measurement.

line turning from lowest to highest ΔN_{leq} values as SRD becomes dominant. For the black line, the intermediate minimum has even vanished and become a shoulder. Whether the recovery from BO-LID in the bulk is complete or not is impossible to say at any injection level.

VII. Experimental Restrictions

Unlike the simulations shown above, the determination of lifetime-equivalent defect densities ΔN_{leq} from experimental data is more restricted. On the one hand, the available injection range Δn is often limited to no more than two decades (e.g., 10^{14}–10^{16} cm^{-3}), implying that only a small part of the characteristic S-shaped p_0-centered $\Delta\tau_{\mathrm{def}}$ or ΔN_{leq} curve of SRH defects is observable. Choosing the doping level p_0 at the upper edge of that range facilitates the ΔN_{leq} determination for deep SRH defects, as $\Delta N_{\mathrm{leq}}(\Delta n)$ increases toward low injection. On the other hand, lifetime measurement uncertainty restricts sensitivity. Consider, e.g., a relative uncertainty $\delta(\tau_{\mathrm{eff}})/\tau_{\mathrm{eff}}$ of 1–8%, which is probably a good estimation for uncertainty in lifetime measurements. Note that uncertainty (by noise) in a measurement typically depends on signal strength linked to injection. This uncertainty will affect both the measured effective lifetimes $\tau_{\mathrm{eff},B}$ before and $\tau_{\mathrm{eff},A}$ after a treatment. How strongly this uncertainty translates to ΔN_{leq}, or better to the relative uncertainty $\delta(\Delta N_{\mathrm{leq}})/\Delta N_{\mathrm{leq}}$, surely depends on how severely the defect-related lifetime $\Delta\tau_{\mathrm{def}}$ limits total effective lifetime τ_{eff} comprising $\Delta\tau_{\mathrm{def}}$ as well as a background lifetime τ_{bg} summing up all other lifetime components. Actually, relative uncertainty of ΔN_{leq} scales with the ratio on $\Delta\tau_{\mathrm{def}}$ / τ_{bg} as it is exemplarily depicted in Fig. 16 for the aforementioned uncertainty range of 1–8%. Uncertainty relates here to the standard deviation of a normal distribution. In general, relative uncertainty of ΔN_{leq} is lowest when $\Delta\tau_{\mathrm{def}}$ is by far lower than τ_{bg} ($\Delta\tau_{\mathrm{def}}/\tau_{\mathrm{bg}} \ll 1$), but even then it is not less than that of the lifetime measurement itself. In contrast, if τ_{bg} is by far lower than $\Delta\tau_{\mathrm{def}}$ ($\Delta\tau_{\mathrm{def}}/\tau_{\mathrm{bg}} \gg 1$), relative uncertainty of ΔN_{leq} increases drastically; the measurement loses its sensitivity to the occurrence of ΔN_{leq}. As a rule of thumb, $\Delta\tau_{\mathrm{def}}$ and τ_{bg} should

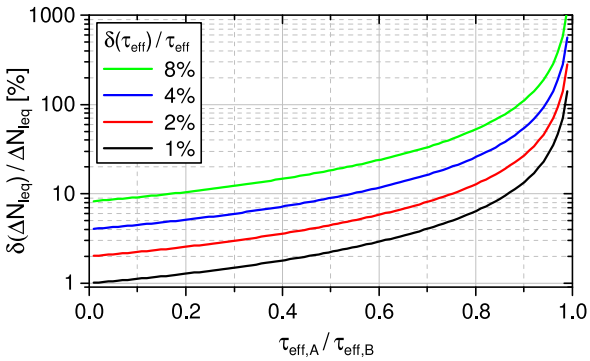

Fig. 17. Relative uncertainty of ΔN_{leq} in dependence of the ratio of effective lifetimes $\tau_{\mathrm{eff},A}$ and $\tau_{\mathrm{eff},B}$ (a) after and (b) before a treatment for various relative uncertainties of the effective lifetime measurement.

at least be balanced to allow for a determination of ΔN_{leq} without sacrificing relative uncertainty compared with τ_{eff}.

However, the $\Delta\tau_{\mathrm{def}}/\tau_{\mathrm{bg}}$ ratio is probably not the easiest accessible parameter in an experiment, where only effective lifetimes $\tau_{\mathrm{eff},B}$ and $\tau_{\mathrm{eff},A}$ are measured. It is found that uncertainty of ΔN_{leq} scales also with the $\tau_{\mathrm{eff},A}/\tau_{\mathrm{eff},B}$ ratio and, thus, independent of the actual value of either $\tau_{\mathrm{eff},B}$ or $\tau_{\mathrm{eff},A}$. The dependence of relative uncertainty of ΔN_{leq} on the $\tau_{\mathrm{eff},A}/\tau_{\mathrm{eff},B}$ ratio is shown in Fig. 17. The closer $\tau_{\mathrm{eff},A}$ and $\tau_{\mathrm{eff},B}$ are to each other and, thus, the lower the observed change in lifetime, the more uncertain ΔN_{leq} becomes. At the latest when relative uncertainty reaches 100%, it becomes from a statistical point of view unclear whether a change in defect density or measurement uncertainty is responsible for the difference in effective lifetime.

In practice, the suggested injection Δn to evaluate ΔN_{leq} depends on how background lifetime depends on injection. If, e.g., τ_{bg} features a rather flat injection dependence toward low injection, e.g., because it resembles a J_0-like surface limitation, and $\Delta\tau_{\mathrm{def}}$ is dominated by a deep SRH defect, evaluating ΔN_{leq} at rather low injection is beneficial with respect to its uncertainty.

VIII. Conclusion

The lifetime-equivalent defect density ΔN_{leq}, also referred to as effective, relative, or normalized defect density, can be used as a direct measure of actual density of a single-defect species changing in between lifetime measurements. However, it is important to note the following.

1) ΔN_{leq} in units of [s^{-1}] should not be confused with actual defect density in units of [cm^{-3}].
2) ΔN_{leq} is by definition related to a change in defect density in between measurements, not to the defect density as a whole, and thus, constant lifetime components cancel out.
3) ΔN_{leq} is injection- and temperature-dependent in contrast with actual defect density, and thus, it should always be clearly stated at which injection and temperature it was determined to allow for proper comparison with others.
4) ΔN_{leq} is only conditionally suited to describe defect systems involving more than one changing defect species. In certain situation, especially if FeB pairing/dissociation occurs, it may even change its sign depending on injection.
5) Exploiting the injection dependence of ΔN_{leq} may offer additional insight into defect dynamics especially in combination with time-resolved analysis.
6) ΔN_{leq} can not only be used to describe defects in the bulk, but in certain situations at the surface as well.
7) Relative uncertainty in ΔN_{leq} depends on how strongly the lifetime component related to ΔN_{leq} impacts effective lifetime as compared with other lifetime components.

References

[1] S. W. Glunz, S. Rein, W. Warta, J. Knobloch, and W. Wettling, "Degradation of carrier lifetime in Cz silicon solar cells," *Sol. Energy Mater. Sol. Cells*, vol. 65, pp. 219–229, 2001. [Online]. Available: https://doi.org/10.1016/S0927-0248(00)00098-2

[2] K. Bothe and J. Schmidt, "Electronically activated boron-oxygen-related recombination centers in crystalline silicon," *J. Appl. Phys.*, vol. 99, 2006, Art. no. 013701. [Online]. Available: https://doi.org/10.1063/1.2140584

[3] B. Lim, F. Rougieux, D. Macdonald, K. Bothe, and J. Schmidt, "Generation and annihilation of boron–oxygen-related recombination centers in compensated p- and n-type silicon," *J. Appl. Phys.*, vol. 108, 2010, Art. no. 103722. [Online]. Available: https://doi.org/10.1063/1.3511741

[4] P. Hamer *et al.*, "Investigations on accelerated processes for the boron-oxygen defect in p-type Czochralski silicon," *Sol. Energy Mater. Sol. Cells*, vol. 145, pp. 440–446, 2016. [Online]. Available: https://doi.org/10.1016/j.solmat.2015.11.013

[5] J. Lindroos and H. Savin, "Review of light-induced degradation in crystalline silicon solar cells," *Sol. Energy Mater. Sol. Cells*, vol. 147, pp. 115–126, 2016. [Online]. Available: https://doi.org/10.1016/j.solmat.2015.11.047

[6] T. Niewelt, J. Schön, W. Warta, S. W. Glunz, and M. C. Schubert, "Degradation of crystalline silicon due to boron–oxygen defects," *IEEE J. Photovolt.*, vol. 7, no. 1, pp. 383–398, Jan. 2017. [Online]. Available: https://doi.org/10.1109/JPHOTOV.2016.2614119

[7] D. Bredemeier, D. Walter, and J. Schmidt, "Light-induced lifetime degradation in high-performance multicrystalline silicon: Detailed kinetics of the defect activation," *Sol. Energy Mater. Sol. Cells*, vol. 173, pp. 2–5, 2017. [Online]. Available: https://.doi.org/10.1016/j.solmat.2017.08.007

[8] D. Chen *et al.*, "Evidence of an identical firing-activated carrier-induced defect in monocrystalline and multicrystalline silicon," *Sol. Energy Mater. Sol. Cells*, vol. 172, pp. 293–300, 2017. [Online]. Available: https://doi.org/10.1016/j.solmat.2017.08.003

[9] T. Niewelt *et al.*, "Understanding the light-induced degradation at elevated temperatures: Similarities between multicrystalline and floatzone p-type silicon," *Prog. Photovolt. Res. Appl.*, vol. 26, pp. 533–542, 2018. [Online]. Available: https://doi.org/10.1002/pip.2954

[10] M. A. Jensen *et al.*, "Evaluating root cause: The distinct roles of hydrogen and firing in activating light- and elevated temperature-induced degradation," *J. Appl. Phys.*, vol. 124, 2018, Art. no. 085701. [Online]. Available: https://doi.org/10.1063/1.5041756

[11] D. Sperber, A. Schwarz, A. Herguth, and G. Hahn, "Bulk and surface-related degradation in lifetime samples made of Czochralski silicon passivated by plasma-enhanced chemical vapor deposited layer stacks," *Phys. Status Solidi A*, vol. 215, 2018, Art. no. 1800741. [Online]. Available: https://doi.org/10.1002/pssa.201800741

[12] D. Sperber, A. Herguth, and G. Hahn, "On improved passivation stability on highly-doped crystalline silicon and the long-term stability of regenerated Cz-Si," *Sol. Energy Mater. Sol. Cells*, vol. 185, pp. 277–282, 2018. [Online]. Available: https://doi.org/10.1016/j.solmat.2018.05.031

[13] A. Herguth and G. Hahn, "Kinetics of the boron-oxygen related defect in theory and experiment," *J. Appl. Phys.*, vol. 108, 2010, Art. no. 114509. [Online]. Available: https://doi.org/10.1063/1.3517155

[14] A. Herguth and B. Hallam, "A generalized model for boron-oxygen related light-induced degradation in crystalline silicon," *AIP Conf. Proc.*, vol. 1999, 2018, Art. no. 130006. [Online]. Available: https://doi.org/10.1063/1.5049325

[15] G. Zoth and W. Bergholz, "A fast, preparation-free method to detect iron in silicon," *J. Appl. Phys.*, vol. 67, no. 11, pp. 6764–6771, 1990. [Online]. Available: https://doi.org/10.1063/1.345063

[16] L. J. Geerligs and D. Macdonald, "Dynamics of light-induced FeB pair dissociation in crystalline silicon," *Appl. Phys. Lett.*, vol. 85, pp. 5227–5229, 2004. [Online]. Available: https://doi.org/10.1063/1.1823587

[17] D. H. Macdonald, L. J. Geerligs, and A. Azzizi, "Iron detection in crystalline silicon by carrier lifetime measurements for arbitrary injection and doping," *J. Appl. Phys.*, vol. 95, pp. 1021–1028, 2004. [Online]. Available: https://doi.org/10.1063/1.1637136

[18] L. J. Geerligs, G. Coletti, and D. Macdonald, "On accurate and quantitative measurements of iron-concentration in multicrystalline silicon by iron-boron pair dissociation," in *Proc. 21st Eur. Photovolt. Sol. Energy Conf.*, Dresden, Germany, 2006, pp. 692–695.

[19] M. Kim *et al.*, "Impact of interstitial iron on the study of meta-stable B-O defects in Czochralski silicon: Further evidence of a single defect," *J. Appl. Phys.*, vol. 123, 2018, Art. no. 161586. [Online]. Available: https://doi.org/10.1063/1.5000323

[20] D. Sperber, A. Graf, D. Skorka, A. Herguth, and G. Hahn, "Degradation of surface passivation on crystalline silicon and its impact on light-induced degradation experiments," *IEEE J. Photovolt.*, vol. 7, no. 6, pp. 1627–1634, Nov. 2017. [Online]. Available: https://doi.org/10.1109/JPHOTOV.2017.2755072

[21] K. Kim *et al.*, "Degradation of surface passivation and bulk in p-type monocrystalline silicon wafers at elevated temperature," *IEEE J. Photovolt.*, vol. 9, no. 1, pp. 97–105, Jan. 2019. [Online]. Available: https://doi.org/10.1109/JPHOTOV.2018.2878791

[22] J. Dziewior and W. Schmid, "Auger coefficients for highly doped and highly excited silicon," *Appl. Phys. Lett.*, vol. 31, pp. 346–348, 1977. [Online]. Available: https://doi.org/10.1063/1.89694

[23] R. A. Sinton and R. M. Swanson, "Recombination in highly injected silicon," *IEEE Trans. Electron Devices*, vol. ED-34, no. 6, pp. 1380–1389, Jun. 1987. [Online]. Available: https://doi.org/10.1109/T-ED.1987.23095

[24] J. Schmidt, M. Kerr, and P. P. Altermatt, "Coulomb-enhanced Auger recombination in crystalline silicon at intermediate and high injection densities," *J. Appl. Phys.*, vol. 88, pp. 1494–1497, 2000. [Online]. Available: https://doi.org/10.1063/1.373878

[25] M. J. Kerr and A. Cuevas, "General parameterization of Auger recombination in crystalline silicon," *J. Appl. Phys.*, vol. 91, pp. 2473–2480, 2002. [Online]. Available: https://doi.org/10.1063/1.1432476

[26] A. Richter, S. W. Glunz, F. Werner, J. Schmidt, and A. Cuevas, "Improved quantitative description of Auger recombination in crystalline silicon," *Phys. Rev. B*, vol. 86, 2012, Art. no. 165202. [Online]. Available: https://doi.org/10.1103/PhysRevB.86.165202

[27] W. Shockley and W. T. Read, "Statistics of the recombinations of holes and electrons," *Phys. Rev.*, vol. 87, pp. 835–842, 1952. [Online]. Available: https://doi.org/10.1103/PhysRev.87.835

[28] R. N. Hall, "Electron-hole recombination in germanium," *Phys. Rev.*, vol. 87, 1952, Art. no. 387. [Online]. Available: https://doi.org/10.1103/PhysRev.87.387

[29] J. D. Murphy *et al.*, "Parameterisation of injection-dependent lifetime measurements in semiconductors in terms of Shockley-Read-Hall statistics: An application to oxide precipitates in silicon," *J. Appl. Phys.*, vol. 111, 2012, Art. no. 113709. [Online]. Available: https://doi.org/10.1063/1.4725475

[30] S. Rein, *Lifetime Spectroscopy—A Method of Defect Characterization in Silicon for Photovoltaic Applications*. Berlin, Germany: Springer, 2005.

[31] S. Rein, T. Rehrl, W. Warta, and S. W. Glunz, "Lifetime spectroscopy for defect characterization: Systematic analysis of the possibilities and restrictions," *J. Appl. Phys.*, vol. 91, pp. 2059–2070, 2002. [Online]. Available: https://doi.org/10.1063/1.1428095

[32] S. Rein and S. W. Glunz, "Electronic properties of the metastable defect in boron-doped Czochralski silicon: Unambiguous determination by advanced lifetime spectroscopy," *Appl. Phys. Lett.*, vol. 82, pp. 1054–1056, 2003. [Online]. Available: https://doi.org/10.1063/1.1544431

[33] J. Schmidt, "Temperature- and injection-dependent lifetime spectroscopy for the characterization of defect centers in semiconductors," *Appl. Phys. Lett.*, vol. 82, pp. 2178–2180, 2003. [Online]. Available: https://doi.org/10.1063/1.1563830

[34] S. Bernardini, T. U. Nærland, A. L. Blum, G. Coletti, and M. I. Bertoni, "Unraveling bulk defects in high-quality c-Si material via TIDLS," *Prog. Photovolt. Res. Appl.*, vol. 25, pp. 209–217, 2017. [Online]. Available: https://doi.org/10.1002/pip.2847

[35] S. Wilking, C. Beckh, S. Ebert, A. Herguth, and G Hahn, "Influence of bound hydrogen states on BO-regeneration kinetics and consequences for high-speed regeneration processes," *Sol. Energy Mater. Sol. Cells*, vol. 131, pp. 2–8, 2014. [Online]. Available: https://doi.org/10.1016/j.solmat.2014.06.027

[36] A. Herguth, C. Derricks, and G. Hahn, "Regeneration of boron-oxygen related degradation in Cz-Si PERC-type solar cells at high temperatures," in *Proc. Eur. Photovolt. Sol. Energy Conf.*, 2017, Amsterdam, The Netherlands, 2017, pp. 557–560. [Online]. Available: https://doi.org/10.4229/EUPVSEC20172017-2AV.1.37

[37] F. Fertig *et al.*, "Mass production of p-type Cz silicon solar cells approaching average stable conversion efficiencies of 22%," *Energy Procedia.*, vol. 124, pp. 338–345, 2017. [Online]. Available: https://doi.org/10.1016/j.egypro.2017.09.308

[38] K. Ramspeck *et al.*, "Light induced degradation of rear passivated mc-Si solar cells," in *Proc. 27th Eur. Photovolt. Sol. Energy Conf.*, Frankfurt, Germany, 2012, pp. 861–865. [Online]. Available: https://doi.org/10.4229/27thEUPVSEC2012-2DO.3.4

[39] F. Fertig, K. Krauß, and S. Rein, "Light-induced degradation of PECVD aluminium oxide passivated silicon solar cells," *Phys. Status Solidi RRL*, vol. 9, pp. 41–46, 2015. [Online]. Available: https://doi.org/10.1002/pssr.201409424

[40] F. Kersten *et al.*, "Degradation of multicrystalline silicon solar cells and modules after illumination at elevated temperature," *Sol. Energy Mater. Sol. Cells*, vol. 142, pp. 83–86, 2015. [Online]. Available: https://doi.org/10.1016/j.solmat.2015.06.015

[41] A. E. Morishige *et al.*, "Lifetime spectroscopy investigation of light-induced degradation in p-type multicrystalline silicon PERC," *IEEE J. Photovolt.*, vol. 6, no. 6, pp. 1466–1472, Nov. 2016. [Online]. Available: https://doi.org/10.1109/JPHOTOV.2016.2606699

[42] A. Herguth, "On the meaning(fullness) of the intensity unit 'suns' in light induced degradation experiments," *Energy Procedia*, vol. 124, pp. 53–59, 2017. [Online]. Available: https://doi.org/10.1016/j.egypro.2017.09.339

[43] F. D. Heinz *et al.*, "The principle of adaptive excitation for photoluminescence imaging of silicon: Theory," *Phys. Status Solidi RRL*, vol. 12, 2018, Art. no. 1800137. [Online]. Available: https://doi.org/10.1002/pssr.201800137

[44] D. Macdonald, J. Tan, and T. Trupke, "Imaging interstitial iron concentrations in boron-doped crystalline silicon using photoluminescence," *J. Appl. Phys.*, vol. 103, 2008, Art. no. 073710. [Online]. Available: https://doi.org/10.1063/1.2903895

[45] A. Y. Liu, Y. C. Fan, and D. Macdonald, "Interstitial iron concentrations across multicrystalline silicon wafers via photoluminescence imaging," *Prog. Photovolt. Res. Appl.*, vol. 19, pp. 649–657, 2011. [Online]. Available: https://doi.org/10.1002/pip.1082

[46] A. Cuevas and D. Macdonald, "Measuring and interpreting the lifetime of silicon wafers," *Sol. Energy*, vol. 76, pp. 255–262, 2004. [Online]. Available: https://doi.org/10.1016/j.solener.2003.07.033

[47] D. E. Kane and R. M. Swanson, "Measurement of the emitter saturation current by a contactless photoconductivity decay method (silicon solar cells)," in *Proc. 18th IEEE Photovolt. Spec. Conf.*, Las Vegas, NV, USA, 1985, pp. 578–583.

[48] A. Kimmerle, J. Greulich, and A. Wolf, "Carrier-diffusion corrected J_0-analysis of charge carrier lifetime measurements for increased consistency," *Sol. Energy Mater. Sol. Cells*, vol. 142, pp. 116–122, 2015. [Online]. Available: https://doi.org/10.1016/j.solmat.2015.06.043

[49] K. R. McIntosh and L. E. Black, "On effective surface recombination parameters," *J. Appl. Phys.*, vol. 116, 2014, Art. no. 014503. [Online]. Available: https://doi.org/10.1063/1.4886595

Axel Herguth received the Diploma degree in physics from the University of Konstanz, Konstanz, Germany, in 2006.

Since 2007, he has been the Head of the characterization group with the Photovoltaics Division, University of Konstanz. His research interests include the kinetics of defects in silicon in general, especially, the kinetic of the boron–oxygen-related defect, as well as characterization techniques for silicon wafers and solar cells.

Mr. Herguth received the Junior Einstein Award from Solarworld in 2006 for his work on the avoidance of the boron–oxygen-related degradation.